Route to high Néel temperatures in 4*d* and 5*d* transition metal oxides

S. Middey,[1] Ashis Kumar Nandy,[1,2] S. K. Pandey,[2] Priya Mahadevan,[2,*] and D. D. Sarma[3,4]

[1]*Centre for Advanced Materials, Indian Association for the Cultivation of Science, Jadavpur, Kolkata-700032, India*

[2]*S. N. Bose National Centre for Basic Sciences, JD-Block, Sector III, Salt Lake, Kolkata-700098, India*

[3]*Solid State and Structural Chemistry Unit, Indian Institute of Science, Bangalore-560012, India*

[4]*Council of Scientific and Industrial Research - Network of Institutes for Solar Energy (CSIR-NISE), New Delhi, India*

(Received 19 December 2011; revised manuscript received 9 July 2012; published 5 September 2012)

There are very few magnetic members among the 4*d* and 5*d* transition metal oxides. In the present work, we examine the recent observation of a high Néel temperature T_N in the 4*d* oxides $SrTcO_3$ and $CaTcO_3$. Considering a multiband Hubbard model, we find that T_N is larger in the limit of a large bandwidth and vanishingly small intra-atomic exchange interaction strength, contrary to our conventional understanding of magnetism. This is traced to specific aspects of the d^3 configuration at the transition metal site and the study reveals additional examples with high T_N.

DOI: 10.1103/PhysRevB.86.104406 PACS number(s): 75.10.−b, 75.47.Lx

I. INTRODUCTION

The picture of magnetism that has prevailed over the years has centered around the existence of localized electrons and their ordering leading to different types of magnetic order. Consequently, one associates the highest magnetic ordering temperatures with the more correlated 3*d* transition metal (TM) oxides, with examples among the 4*d* and 5*d* oxides that have wider bands, more a rarity than the norm. It was therefore a surprise when recently high antiferromagnetic (AFM) ordering temperatures (T_N) of 1023 and 800 K were found in 4*d* TM oxides $SrTcO_3$[1] and $CaTcO_3$,[2] respectively. These were much higher than any of their 3*d* counterparts ($SrMnO_3$; $T_N = 233$ K).[3] In a short span, these unexpected experimental observations have generated a lot of theoretical interest and several possible explanations were offered.[1,4,5] One reason was the smaller Hund's coupling strength and the larger bandwidth associated with the 4*d* oxides.[1] However, within a picture of itinerant magnetism that one has so far, both these correspond to effects which should result in a reduction in the magnetic ordering temperatures and so the puzzle remains. An alternate explanation offered by Georges and coworkers was that $SrTcO_3$ sits at the boundary between the itinerant to localized regime and hence has such a high transition temperature.[5] If this was the case, then one should have several examples among 4*d* and 5*d* oxides with large magnetic ordering temperatures. Looking for other candidate systems, one finds some patterns. The 5*d* oxide $NaOsO_3$ shows a Curie-Weiss metallic nature at high temperature and suddenly goes into an antiferromagnetically insulating state at 410 K on cooling.[6] It has been further confirmed very recently using neutron and x-ray scattering[7] that the metal-insulator transition in $NaOsO_3$ coincides with the onset of long-range commensurate three dimensional magnetic order and thus $NaOsO_3$ is a perfect example of a Slater insulator.[8] The antiferromagnetic ordering temperature (117 K)[9] for another 5*d* material Ca_3LiOsO_6 is much larger compared to analogous 3*d* oxide Ca_3ZnMnO_6 ($T_N = 26$ K).[10]

Considering all these examples that one has identified, a common feature emerges. All these represent systems with a d^3 configuration at the transition metal site, and each identified case corresponds to a half-filling of the t_{2g} bands. This suggests that the filling at the transition metal site is a strong determining factor whether a particular 4*d*/5*d* oxide will have a high magnetic ordering temperature or not.

In this work, we reexamine the issue of a high T_N that has been observed in the examples given above. First-principles electronic structure calculations carried out within the framework of density functional theory reproduce the experimental trends and find large stability for the G-type antiferromagnetic[11] state in all these systems, consistent with earlier reports. However, the microscopic reasons why a large magnetic stability is found still remains a puzzle as the 4*d* and 5*d* oxides have wider bands than their 3*d* counterparts. This makes moment formation less possible and, indeed, one finds very few members of these series that are magnetic. So when even the presence of a local moment is difficult, the large Néel temperatures found in each case are enigmatic. In order to understand this further, we calculated the phase diagram in the U-Δ plane starting with the tight-binding parameters relevant for $SrTcO_3$, as the Coulomb interaction U as well as the charge transfer energy Δ between the transition metal and the oxygen are the dominant parameters that determine the properties of oxides.[12,13] Surprisingly, a small value of U of just 0.6 eV is found to allow a magnetic moment to be sustained. This is traced to the half-filling of the t_{2g} levels that results in a band gap opening up for a small value of U for the antiferromagnetic (AFM) state, associated with the nesting of the Fermi surface. This is in contrast to what one expects for a wide band material where the more efficient screening decreases the coulomb interaction strength and makes the formation of local moments difficult. While a magnetic moment is stabilized even for small U in the G-AFM[11] state, one finds that other magnetic solutions are able to sustain a magnetic moment only at larger values of U.

In the insulating state, there are channels present for the electrons to delocalize and lower their energy only in the AFM state. This energy lowering which strongly stabilizes the G-AFM state is larger for small intra-atomic exchange interaction strength (J_h) as well as large hopping strength and exists even in the limit of a vanishingly small J_h. The metal-insulator transition for a ferromagnetic (FM) state takes

place at a larger value of U than the G-AFM state. So, although there are channels for delocalization present in the FM metallic state, these are smaller than the G -AFM state and vanish as U is increased and the system becomes insulating. As a result the exchange interaction strength (J_0) among the spins increases with U for small values of U and decreases with U in the large U region. As the energy gain by delocalization for the G-AFM state decreases from 5d to 4d to 3d TM compounds, one expects a similar trend in the T_N. Although the T_N does increase from $SrMnO_3$ to $SrTcO_3$, $NaOsO_3$ is found to have a lower Néel temperature. This is because the T_N depends on aspects of the relevant electronic interaction strengths. Our calculations predict that there should be other examples among the 5d oxides with higher Néel temperatures. The high T_N, we find, is a generic feature of all 4d and 5d oxides with a d^3 configuration (half-filled t_{2g} band), and we extend this class of high T_N oxides to include Sr_2TcO_4, Ca_2TcO_4, $Sr_3Tc_2O_7$, Li_2TcO_3, $NaOsO_3$, and Ca_3LiOsO_6.

II. METHODOLOGY

The electronic and magnetic structure of $SrTcO_3$ for the experimentally observed orthorhombic structure[1] has been calculated within a plane-wave pseudopotential implementation of density functional theory using PAW potentials[14] as implemented in VASP.[15] We have performed several GGA + U calculations where the U was varied from 0, 2, and 3 eV on Tc consistent with the estimate for Ru[16] as well as a recent estimate for $SrTcO_3$.[17] A k mesh of $6 \times 6 \times 6$ was used with a plane-wave cutoff energy of 400 eV. In order to understand the origin of the observed magnetic stability and its dependence on microscopic parameters, we have carried out an additional analysis in terms of a multiband Hubbard-like Hamiltonian given by Eq. (1):

$$\begin{aligned} H = & \sum_{i,l,\sigma} \epsilon_p p^\dagger_{il\sigma} p_{il\sigma} + \sum_{i,l,\sigma} \epsilon^l_d d^\dagger_{il\sigma} d_{il\sigma} \\ & - \sum_{i,j,l_1,l_2,\sigma} \left(t^{l_1 l_2}_{i,j,pp} p^\dagger_{il_1\sigma} p_{jl_2\sigma} + \text{H.c.} \right) \\ & - \sum_{i,j,l_1,l_2,\sigma} \left(t^{l_1 l_2}_{i,j,pd} d^\dagger_{il_1\sigma} p_{jl_2\sigma} + \text{H.c.} \right) \\ & + \sum_{\alpha\beta\gamma\delta,\sigma_1\sigma_2\sigma_3\sigma_4} U^{\alpha\beta\gamma\delta}_{dd} d^\dagger_{\alpha\sigma_1} d^\dagger_{\beta\sigma_2} d_{\gamma\sigma_3} d_{\delta\sigma_4}, \end{aligned} \quad (1)$$

where $d^\dagger_{il\sigma}(d_{il\sigma})$ creates (annihilates) an electron with spin σ in the lth d orbital on T_c in the ith unit cell, $p^\dagger_{im\sigma}(p_{im\sigma})$ creates (annihilates) an electron with spin σ in the mth p orbital on oxygen atom in the ith unit cell. The parameters entering the tight-binding part of the Hamiltonian are determined by fitting the *ab initio* band structure for the nonmagnetic case to a tight binding model that included s and p states on oxygen and d states on Tc. Hopping is included between Tc d and O s as well as p states as well as between the p states on oxygen atoms and these [t_{ij}'s in Eq. (1)] are parameterized in terms of the Slater-Koster parameters $pd\sigma$, $pd\pi$, $sd\sigma$, $pp\sigma$, and $pp\pi$.[18] The semicore O s states were included to simulate the splitting between the Tc states with t_{2g} and e_g symmetry at Γ point.[19]

In addition, we also include Coulomb interactions between electrons on the Tc site. This ($U^{\alpha\beta\gamma\delta}_{dd}$) is parameterized in terms of the Slater-Condon integrals[20] F^0, F^2, and F^4. The values of these are obtained from atomic Hartree-Fock calculations though F^0 is substantially screened due to solid state effects. Usually, F^0 is chosen to result in an appropriate multiplet averaged Coulomb interaction strength defined as U in the present case. F^2 and F^4 are scaled to 80% of their values in describing 3d transition metal compounds. The reduction is again to account for screening effects in solids. As F^2 and F^4 are related to the intra-atomic exchange interaction strength, in the present case, we have scaled them to lead to a desired value of the intra-atomic exchange interaction strength J_h; similar to the earlier approaches for the calculation of the spectral functions corresponding to photoemission spectroscopies, x-ray absorption spectroscopies, etc.[21] A mean-field decoupling scheme is used for the four Fermion terms and the order parameters are solved self-consistently.[12] This allowed us the freedom of calculating the variations in electronic and magnetic properties as a function of J_h. The total energies were determined for ferromagnetic as well as A-type, C-type, and G-type antiferromagnetic configurations. A schematic diagram for each of the antiferro configurations is given in Fig. 1. It should be noted that the number of antiferromagnetic first-neighbor Tc atoms increases as the antiferromagnetic configuration changed from A to C to G type. The energies for the different magnetic configurations were then mapped onto a Heisenberg spin model ($-\frac{1}{2}\sum J_{ij}\ \mathrm{S}_i.\mathrm{S}_j$ where $|\mathrm{S}_i| = 3/2$) with first neighbor (J_1) as well as second neighbor (J_2) exchange interaction strengths. Here, the unit vector e_i denotes the direction of the spin at the ith site. An effective exchange

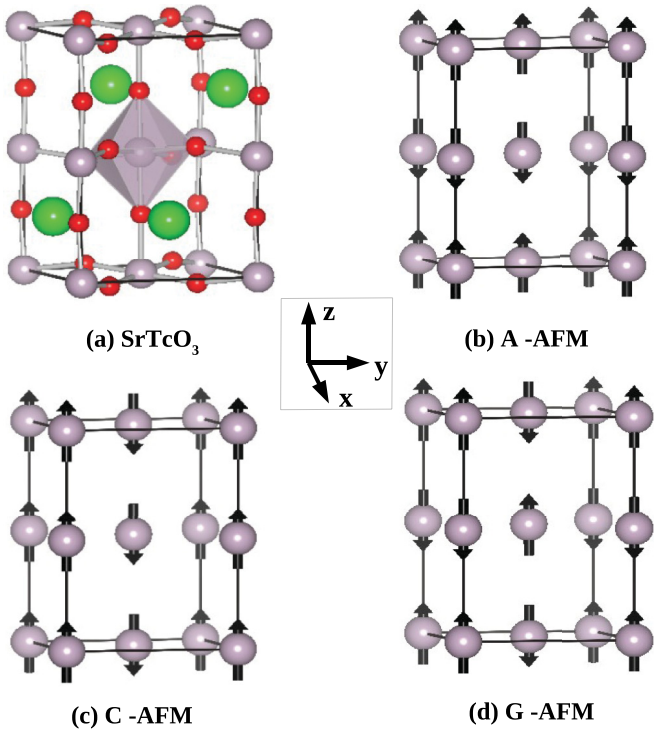

FIG. 1. (Color online) $SrTcO_3$ (a) crystal structure (b) A (c) C, and (d) G-type antiferromagnetic configurations. Large green, medium gray, and small red spheres in (a) are Sr, Tc, and O atoms, respectively. Black arrows in (b)–(d) denote the spins on the Tc sites for different antiferromagnetic configurations.

TABLE I. Stabilization energy (meV/f.u.) for $SrTcO_3$ with respect to the nonmagnetic state from GGA + U calculations.

U(eV)	Ferro	A-AFM	C-AFM	G-AFM
0	nonmag	nonmag	−46	−168
2	−432	−568	−662	−745
3	−925	−1029	−1100	−1164

interaction strength J_0 given by $6J_1 + 12J_2$ was determined as this is directly related to T_N in a mean-field model, up to a multiplicative constant. For the values of the interaction strengths believed to be relevant for $SrTcO_3$ and $SrMnO_3$, we have used the extracted values of J_1 and J_2 to calculate T_N using a Monte Carlo simulation (MC).[22] During an MC run, one considers a lattice site i with a random orientation $\mathbf{e}_i$ of the magnetic moment. One then creates a new random orientation $\mathbf{e}_i'$ and decides by looking at the system energy whether $\mathbf{e}_i'$ lowers the system energy or not. If the energy is lowered then one accepts $\mathbf{e}_i'$, else we use the metropolis algorithm[23] to decide whether $\mathbf{e}_i'$ is kept. We have performed this procedure for a $16 \times 16 \times 16$ lattice for each MC step. Starting from a random spin configuration the system is brought into a thermal equilibrium within 2×10^5 MC steps for every temperature cycle. Once the system goes into the thermal equilibrium, we have calculated the magnetization in each sublattice. This has been used to determine T_N. As the results can be sensitive to finite size effects, we checked for convergence with respect to the lattice sites and found that at the sizes used we were converged.

III. RESULTS AND DISCUSSIONS

The total energies referenced to the nonmagnetic state for different magnetic configurations (Ferro, A-FM, C-AFM, G-AFM)[11] determined from our *ab initio* calculations are given in Table I. As observed earlier,[1] the FM and A-AFM calculations converge to a nonmagnetic solution for $U = 0$. Surprisingly, the magnetic structures in which each Tc atom has more AFM neighbors are the ones that converge to a magnetic solution. This was also found earlier and a possible reason was attributed to a need for beyond-LDA effects due to the incorrect treatment of the residual exchange-correlation effects.[4] Correcting for this with hybrid functionals (HSE06), they were able to examine all magnetic solutions and discuss trends in T_N for the series $ATcO_3$, where $A =$ Ca, Sr, Ba. Using a computationally less intensive method, GGA + U we are able to converge to magnetic solutions for all configurations. Apart from the robustness of the G-AFM ground state, we also find a larger stability for the G-AFM state over the FM state for $U = 2$ than for $U = 3$ eV.

The reasons for observed trends in first-principles calculations are usually difficult to pinpoint as a result of being dependent on several parameters, which need not be the same as U is varied. In order to carry out a microscopic analysis to understand the origin of magnetic ordering, we set up a multiband Hubbard-like model for $SrTcO_3$ with a U on Tc. A least squared error minimization procedure was used to estimate the best set of parameters entering the tight-binding part of the Hamiltonian that best fit the *ab initio* band structure.[24] The bands with primarily Tc d character as well as the O p nonbonding states were included in the fitting. The *ab initio* band structure is plotted in Fig. 2(a) with the corresponding tight-binding band structure obtained with the best fit parameters plotted in Fig. 2(b). To compare with the corresponding $3d$ oxide $SrMnO_3$, the tight-binding parameters also have been found in a similar way for $SrMnO_3$ and compared in Table II. The main differences in going from $3d$ to $4d$ oxides are the increase of crystal field splitting, as evidenced by a change in $sd\sigma$. As expected one also has an increase of hopping interaction strength between the transition metal d and oxygen p orbital due to increase of spatial extent of the d orbitals in going from $3d$ to $4d$. The charge transfer energy Δ on the other hand remains similar.

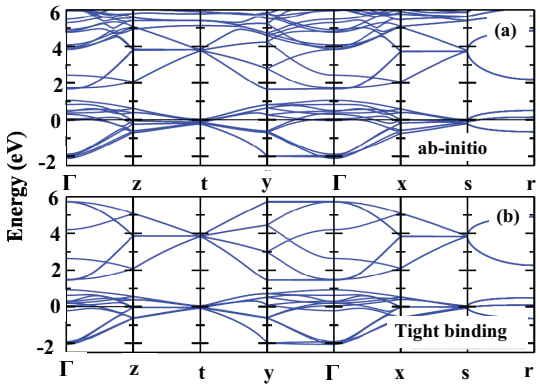

FIG. 2. (Color online) (a) The *ab-initio* and (b) tight-binding band dispersions for $SrTcO_3$ along different symmetry directions. The parameters entering the tight-binding Hamiltonian are determined by a least-square error minimization fit of the *ab initio* band dispersions.

After obtaining the hopping parameters, we solve the multiband Hubbard-like model for $SrTcO_3$ with U on Tc for several values of U and Δ (charge transfer energy). Features of the solutions observed earlier in the context of the *ab initio* calculations are observed here also. While the G-type AFM solution is found to be robust, the existence of the other magnetic solutions depends on the value of U. Examining the different solutions at $\Delta = 2$ eV and a small value of U equal to 0.6 eV, we find that only the G-AFM solution exists, while all other magnetic solutions converge to a nonmagnetic solution. Examining the Tc d and O p partial density of states (DOS) [see Fig. 3(a)], we find that the t_{2g} states with primarily Tc d character are almost 3 eV wide. As a consequence of Fermi surface nesting at half-filling,[25] a band gap opens up for just $U = 0.6$ eV and $J_h = 0.1$ eV

TABLE II. Slater Koster parameters (in eV) for $SrTcO_3$ and $SrMnO_3$ determined from a tight-binding analysis (see Ref. 24).

Parameter	$SrMnO_3$	$SrTcO_3$
$pp\sigma$	0.75	0.60
$pp\pi$	−0.10	−0.15
$sd\sigma$	−2.55	−3.40
$pd\sigma$	−2.20	−3.30
$pd\pi$	1.15	1.55
E_d-E_p	1.40	2.0

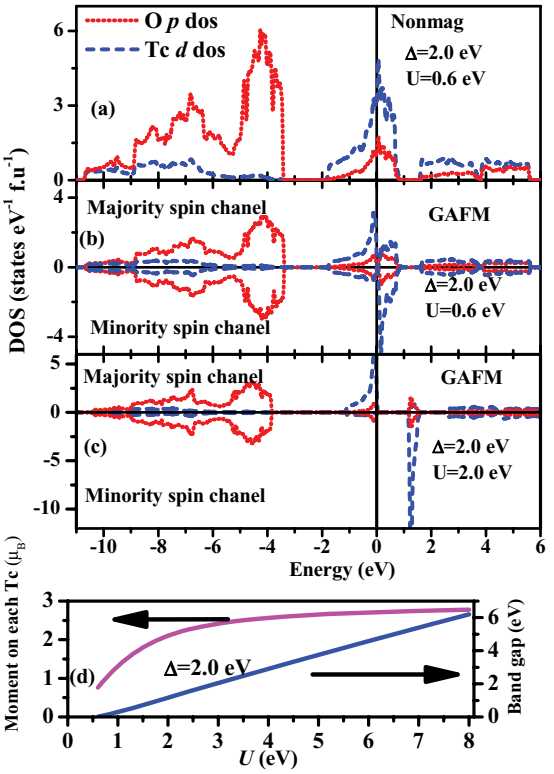

FIG. 3. (Color online) Partial density of states of Tc d and O p states in $SrTcO_3$ for (a) nonmagnetic solution of a multiband Hubbard model with $\Delta = 2.0$ eV, $U = 0.6$ eV; (b) G-AFM spin configuration with $\Delta = 2.0$ eV, $U = 0.6$ eV; (c) G-AFM spin configuration with $\Delta = 2.0$ eV, $U = 2.0$ eV for majority [upper part of (b) and (c)] and minority [lower part of (b) and (c)] spins. The variations of band gap as well as magnetic moment on Tc with U are plotted in (d) for $\Delta = 2.0$ eV.

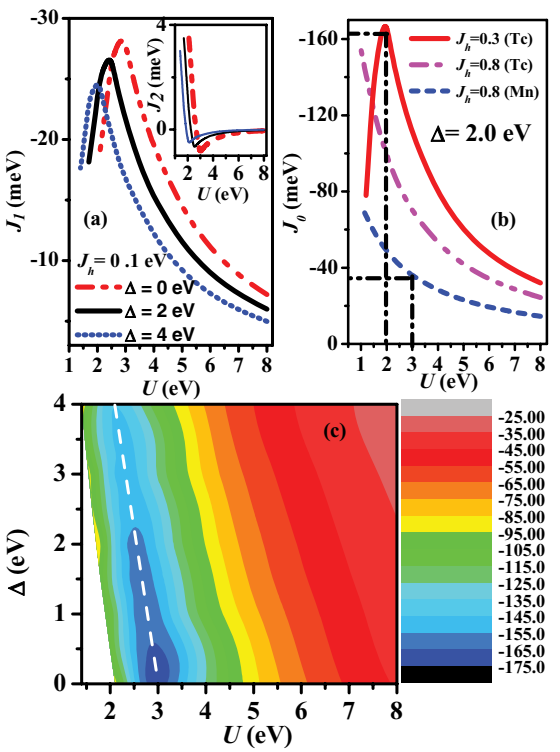

FIG. 4. (Color online) (a) The variation of J_1 with U for $\Delta = 0$, 2, 4 eV calculated within a multiband Hubbard model. The inset shows the corresponding variation of J_2. (b) J_0 as a function of U for $J_h = 0.3$, 0.8 for $SrTcO_3$ and 0.8 eV for $SrMnO_3$. (c) Contour plot of J_0 in the U-Δ plane for $SrTcO_3$ with $J_h = 0.1$ eV. The dotted line indicates the position of maxima of J_0.

for the G-AFM configuration [see Fig. 3(b)]. This increases to 1.1 eV when U is increased to 2 eV [see Fig. 3(c)], scaling almost linearly with U as shown in Fig. 3(d). Once the system goes insulating, it can very easily sustain a local magnetic moment as the hopping processes between the majority spin t_{2g} states at one site and the unoccupied minority spin t_{2g} states at the neighboring site helps the stability of the AFM state. The variation of the magnetic moment in the G-AFM configuration at each Tc site is plotted as a function of U in Fig. 3(d). The magnetic moment is found to increase from a value of 0.6 μ_B at $U = 0.6$ eV to an almost saturation value of 2.5 μ_B at $U = 3$ eV, in contrast to a fully ionic value of 3 μ_B. These values give a sense of the itinerant nature of the magnetism. For the FM case or the other AFM configurations where some neighboring spins are aligned ferromagnetically, the metal-insulator transition takes place at a larger value of U. Once these solutions become insulating, the channel for delocalization between every ferromagnetically aligned pair of spins is lost. This explains the robustness of the G-AFM solution in regions of the parameter space where the other magnetic solutions converge to nonmagnetic solutions.

Two key parameters that control the properties of TM oxides are Δ and U. To check the stability of the magnetic state of $SrTcO_3$, we have calculated the interatomic exchange interaction strengths J_i's by mapping onto a Heisenberg model with different combinations of Δ and U with $J_h = 0.1$ eV. Inspite of deviations of the magnetic moment from the ionic value for a given set of U and Δ, we found that the variations between different magnetic configurations was 10% or lower. This justifies the mapping onto a spin only model. The variations in J_1 and J_2 as a function of U for three values of Δ equal to 0, 2, and 4 eV are shown in Fig. 4(a). As the G-AFM is found to be the lowest-energy solution for all values of Δ, J_1 turns out to be AFM while J_2 [inset of Fig. 4(a)] is primarily FM. Considering the case of $\Delta = 4$, we find that the magnitude of J_1 first increases, and then decreases as U is increased. The magnitude of J_2 decreases over a small U variation and may then be approximated to 0. As J_2 involves higher order hopping processes, its value is finite only when the hopping interaction strength is sizable (i.e., the small U regime). As J_0 is dominated by J_1, we discuss the variation in J_1 that we find in order to understand the dependence of T_N on microscopic interaction strengths. We are not able to extract J_i's in the region where only some of the configurations converge to magnetic solutions.

A simple perturbative treatment of the energies was carried out considering a fully spin-polarized ground state at each TM site and the allowed first excited state. This simple model is able to capture the basic physics of why J_1 goes through a maximum as a function of U. In this limit, there are no delocalization pathways for a FM arrangement, the energy gain for the AFM arrangement is directly related to J_1. In the low U limit, where U is the perturbation, we find that J_1 varies as U.

In the large U limit, treating the hopping as a perturbation results in J_1 varying as $1/U$. It is immediately clear that this would imply that J_1 should go through a maximum as a function of U and this is indeed what is observed in Fig. 4(a) for various values of Δ studied. The largest J_1 is seen for the smallest Δ as the effective hopping between the sites will be the largest there.

In order to probe the role of J_h, we have calculated J_0 for two values of J_h; a value of 0.3 eV,[26] as well as a typical value of 0.8 eV for $SrTcO_3$ and $SrMnO_3$ and plotted them in Fig. 4(b). Although the J_0 variation shows the same trend for both values of J_h, there is a dramatic reduction in J_0 in going from J_h of 0.3 to 0.8 eV. This stems from the fact that the effective exchange splitting approximately varies as $U + 2J_h$. This goes into the denominator of the effective hopping interaction strength that determines J_1, explaining the observed reduction. Similar trends are seen for $SrMnO_3$ for which we show the variation in J_0 only for $J_h = 0.8$ eV. If a U of 3 eV is believed to be appropriate, for $SrMnO_3$ and a slightly reduced value of 2 eV seems likely for $SrTcO_3$, the ratio of the calculated J_0's and therefore T_N's are in the ratio 4 : 1, with that for $SrTcO_3$ being higher and consistent with experiment. The calculated J_1 and J_2 are used in a Monte Carlo code to calculate the finite temperature magnetic moment of one sublattice for $SrMnO_3$ as well as $SrTcO_3$. These are shown in Fig. 5. The calculated Néel temperatures are found to be 230 and 1015 K, respectively, in very good agreement with the experimental values. The mapping onto a localized spin model in the context of a 4*d* oxide, which has wide bands is indeed questionable. In order to examine, this we compared the variation of Tc moment in one sublattice with what is known experimentally[27] (see Fig. 5). In contrast to what is known in the literature for itinerant magnets,[28] the agreement in the present case is very good, ratifying the mapping. This is possibly because the insulating character of the ground state, kills the longitudinal spin wave fluctuations seen in metallic systems that cause a deviation from a Heisenberg-like behavior.

The values of J_0 have been extracted in the complete U-Δ plane, and plotted in Fig. 4(c). The largest values of J_0 are

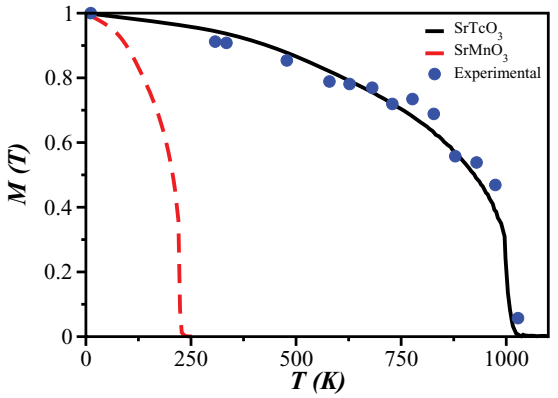

FIG. 5. (Color online) The variation of the magnetic moment as a function of temperature (T) for $SrTcO_3$ and $SrMnO_3$ calculated within a Heisenberg model with nearest neighbor (J_1) and next-nearest-neighbor (J_2) exchange interactions. The experimental variations (solid circle) for the saturation magnetic moment from Ref. 27 are provided for $SrTcO_3$.

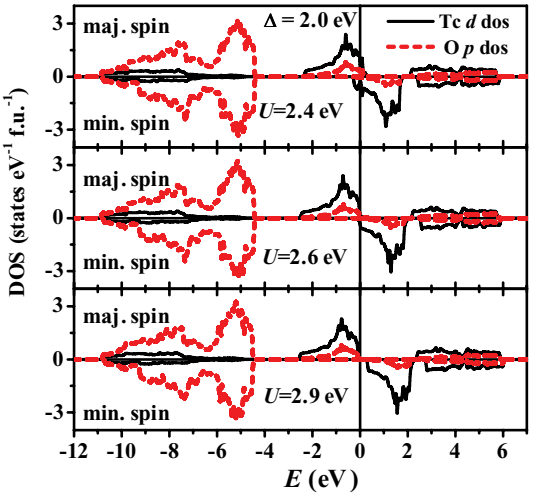

FIG. 6. (Color online) Majority and minority spin partial density of states for Tc *d* and O *p* calculated for ferromagnetic configuration with $\Delta = 2$ eV and U varied from 2.4 to 2.9 eV calculated within a multiband model for $SrTcO_3$. The band gap is just opening near $U = 2.6$ eV and is clearly visible at $U = 2.9$ eV.

seen near $U = 3$ eV for small Δ (~0.3 eV). As a function of U, they are found to occur about the dashed line drawn with a slight slope to the line $U = 3$. There are two dominant energetics which determine the magnitude of J_0. The first is the delocalization channels present in the AFM arrangement and the second are the delocalization channels present in the FM metallic state. As a result of nesting, while the AFM solution goes insulating at small values of $U = 0.6$ eV, for $\Delta = 2.0$ eV, the FM solution remains metallic upto a value of U equal to 2.5 eV (see Fig. 6), which is of the order of the bandwidth. Hence depending on the magnitude of the effective hopping parameter, one could be in a regime where the peak is close to the point where the FM solution goes insulating or far from it.

The results of Fig. 4 indicate a wide parameter regime for the stability of the G-AFM state as the ground state, thereby suggesting that the large magnetic stabilization energies are not limited to just $SrTcO_3$ and $CaTcO_3$, but is generic of all TM oxides with a d^3 configuration/half-filling of the t_{2g} band. This motivated us to examine the magnetic ground state for other Tc-based compounds analogous to the layered, bilayer ruthenates. Unfortunately, those compounds Sr_2TcO_4, Ca_2TcO_4, $Sr_3Tc_2O_7$, etc., have so far not been synthesized. The structural information for another Tc oxide, Li_2TcO_3 was also reported long back,[29] though the magnetic property is still unknown. The electronic and the magnetic structure of above mentioned compounds have been calculated using VASP[15] with GGA form for the exchange correlation functional. The starting structure for Li_2TcO_3 was taken from the literature.[29] For the other compounds, the structure of the analogous

TABLE III. Stabilization energy for $Sr_3Tc_2O_7$ (meV/Tc) with respect to the nonmagnetic state and magnetic moment M (in μ_B) on each Tc for G-AFM state.

U(eV)	Ferro	A-AFM	C-AFM	G-AFM	M for G-AFM
$Sr_3Tc_2O_7$	nonmag	−3	−110	−163	1.65

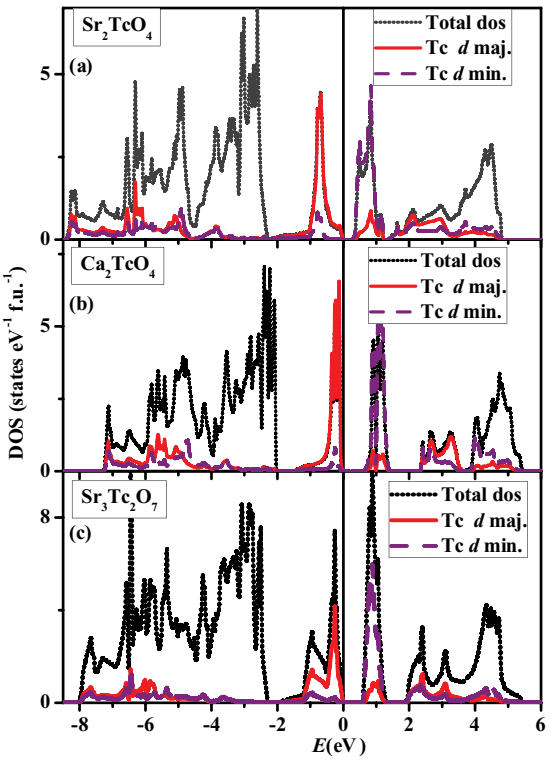

FIG. 7. (Color online) Total DOS and majority and minority spin Tc d partial dos for antiferromagnetic configuration of (a) Sr_2TcO_4, (b) Ca_2TcO_4, and (c) $Sr_3Tc_2O_7$. The zero in energy denotes E_F in every case.

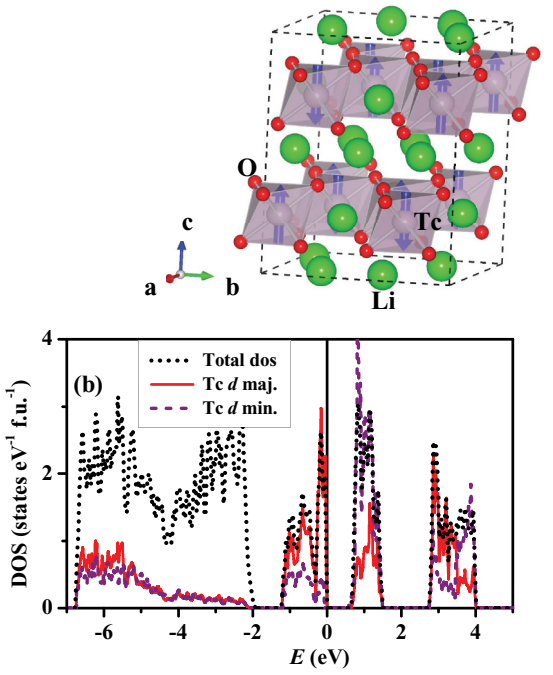

FIG. 8. (Color online) (a) Antiferromagnetic spin arrangement in Li_2TcO_3. (b) Total DOS and Tc d partial dos for majority and minority spin channels.

Ru compounds[30–32] was taken. This is because the crystal structure of $SrTcO_3$ ($CaTcO_3$) is very similar to that of $SrRuO_3$ ($CaRuO_3$) and so one expects the other Tc compounds to be similar. In these calculations, the lattice constants were kept fixed, while the internal coordinates were reoptimized in order to minimize the total energy.

The stabilization energies for different spin configurations with respect to the nonmagnetic state are listed in Table III for bilayer compound $Sr_3Tc_2O_7$, where each TcO_6 octahedra is coordinated with 4 (1) such octahedra in ab plane (along c direction).[30] Similar to $SrTcO_3$, the magnetic configuration in which each Tc atom has more number of antiferromagnetic neighbors are the ones which converge to a magnetic solution. The stabilization energy of G-AFM state when compared to the C-AFM state is found to be -53 meV/Tc, which is almost half of the stabilization energy found for $SrTcO_3$. This can be understood in terms of the modified connectivity. The magnitude of magnetic moment is found to be 1.65 μ_B which is substantially smaller than the full ionic moment of 3 μ_B. This reduction is due to the strong covalency interaction between Tc d and O p orbital. The DOS [see Fig. 7(c)] for the G-AFM state is strongly modified from the nonmagnetic one by magnetic ordering, and a small band gap of 0.6 eV is found. So, *ab initio* analysis suggests that similar to $SrTcO_3$, the bilayer $Sr_3Tc_2O_7$ will also be antiferromagnetic with a high T_N.

In the next attempt, we took the single layered compounds Sr_2TcO_4 and Ca_2TcO_4 where the superexchange pathways between Tc sites exist only in the ab plane. Here, two possible magnetic configurations were considered: ferro and AFM where each Tc is connected ferromagnetically or antiferromagnetically with the four Tc atoms in the basal plane. The magnetic stabilization energies with respect to the nonmagnetic state are given in Table IV. Only the AFM solution converges to a magnetic solution and this is found to be stable by 125 meV/Tc over the nonmagnetic solution. In Sr_2TcO_4, the DOS which is plotted [see Fig. 7(a)] for G-AFM configuration shows that it is also insulating with a smaller band gap of 0.3 eV. For Ca_2TcO_4, the AFM state is stabilized over the ferromagnetic state by -194 meV/Tc. The ferromagnetic state was found to be metallic, where as the AFM state is insulating with a band gap of 0.6 eV [see Fig. 7(b)]. So, strong antiferromagnetic and insulating states are also obtained as ground states in these single layered

TABLE IV. Stabilization energy (meV/Tc) with respect to the nonmagnetic state and magnetic moment M (in μ_B) on each Tc for AFM state.

U(eV)	Ferro	AFM	M for G-AFM
Sr_2TcO_4	nonmag	-125	1.55
Ca_2TcO_4	-96	-290	1.85
Li_2TcO_3	nonmag	-110	1.15

TABLE V. Stabilization energies (meV/f.u.) for $NaOsO_3$ with respect to the nonmagnetic state.

U(eV)	Ferro	A-AFM	C-AFM	G-AFM
0	nonmag	nonmag	nonmag	-20
1	-7	-11	-50	-127
3	-295	-415	-521	-587

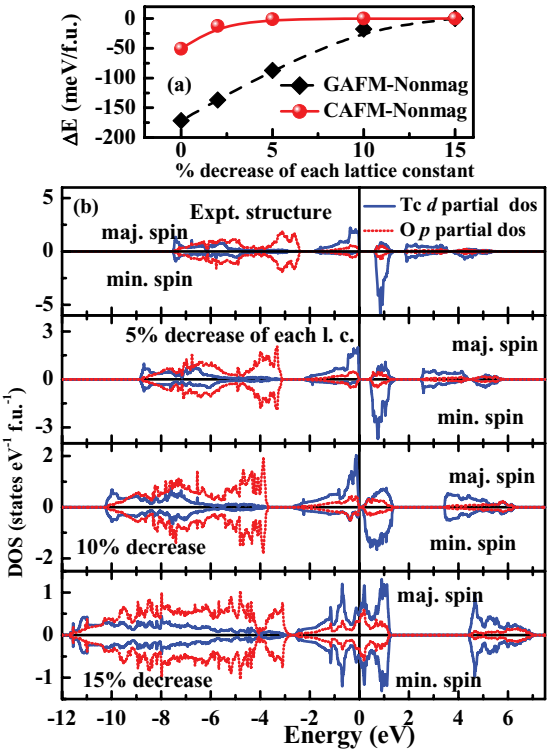

FIG. 9. (Color online) (a) The variation in the magnetic stabilization energy for G-AFM and C-AFM configurations plotted as a function of the percentage decrease in each lattice constant. (b) Tc *d* and O *p* contributions to the density of states for G-AFM configurations for different isotropic compressions of the lattice constants. At a 15% decrease of all the lattice constants, the G-AFM solution turns nonmagnetic.

Tc oxides. The magnetic moments on Tc were found to be 1.55 μ_B and 1.85 μ_B for Sr_2TcO_4 and Ca_2TcO_4, respectively.

Li_2TcO_3 has a monoclinic structure with space group of $C2/c$. Figure 8(a) shows that each TcO_6 unit is connected with another adjacent octahedra sharing a common edge and there are three such coordinations for each octahedra in the basal plane. Such two-dimensional units are separated from each other along the c axis by an intermediate Li-O layer. Here, the smaller Tc-Tc separation (2.9 Å) also gives the possibility of direct Tc-Tc interaction. In spite of the significant structural differences from the previously discussed members of the $A_{n+1}Tc_nO_{3n+1}$ family (A = Sr/Ca, n = 1, 2, ∞), one finds that the antiferromagnetic state is the ground state here also with a stabilization energy of −110 meV/Tc. This is also insulating with a band gap of 0.6 eV [see Fig. 8(b)].

The analysis for the Tc compounds has resulted in large stabilization energies for several as yet unexplored examples in addition to establishing this as a generic feature of all d^3 compounds. Moving to the 5*d* compounds one finds that $NaOsO_3$ has a large Néel temperature of 410 K. This seems to be surprisingly large considering that most examples among the 5*d* oxides have magnetic ordering temperatures of the order of few K. The energies calculated for different magnetic configurations are given in Table V. Here, again large stabilization energies are obtained.

Another probe that could be used in experiments is hydrostatic pressure, which could be used to examine the stability of the G-AFM ground state. Evaluating the total energy differences between the G and the C-AFM ground states within *ab initio* GGA based calculations using the $SrTcO_3$ structure as a starting point, we find that with a small change in the lattice constant of 2.5%, the C-AFM solution is no longer stable and converges to a nonmagnetic solution [see Fig. 9(a)]. The G-AFM solution we find is stable and as revealed by the total energy difference with the nonmagnetic state plotted in Fig. 9(a) as well as the Tc *d* and O *p* projected partial density of states plotted in Fig. 9(b) for 0, 5, 10, and 14% decrease in the lattice parameter. For a lattice parameter change larger than 10%, we find a collapse of the G-AFM solution to the nonmagnetic solution, again supporting the robustness of the G-AFM solution.

IV. CONCLUSIONS

We have examined the origin of a high T_N in $SrTcO_3$ as well as other Tc compounds with a half filling of the t_{2g} bands within *ab initio* calculations. This is supplemented in some cases by an analysis within the mean-field limit of a multiband Hubbard-like model. A wide range of parameters is found for which the G-AFM solution is stable. In contrast to usual expectations, the magnetic stabilization energy is found to be larger in the limit of small J_h and larger bandwidths. This is traced to aspects of the d^3 configuration at the TM site, which in the insulating state, allows electrons to delocalize only in the AFM configuration. Using the appropriate values of the interaction strengths for $SrTcO_3$, we get a T_N of 1015 K, which is four times larger than that for $SrMnO_3$, in agreement with experiments.

ACKNOWLEDGMENT

SM, AKN, thank CSIR, India for fellowship. DDS and PM thank the Department of Science and Technology, India. Part of the work is supported by the European Union FP7 program and the Department of Science and Technology under the Indo-EU project ATHENA.

*Corresponding author: priya@bose.res.in

[1]E. E. Rodriguez, F. Poineau, A. Llobet, B. J. Kennedy, M. Avdeev, G. J. Thorogood, M. L. Carter, R. Seshadri, D. J. Singh, and A. K. Cheetham, Phys. Rev. Lett. **106**, 067201 (2011).

[2]M. Avdeev, G. J. Thorogood, M. L. Carter, B. J. Kennedy, J. Ting, D. J. Singh, and K. S. Wallwork, J. Am. Chem. Soc. **133**, 1654 (2011).

[3]O. Chmaissem, B. Dabrowski, S. Kolesnik, J. Mais, D. E. Brown, R. Kruk, P. Prior, B. Pyles, and J. D. Jorgensen, Phys. Rev. B **64**, 134412 (2001).

[4]C. Franchini, T. Archer, J. He, Xing-Qiu Chen, A. Filippetti, and S. Sanvito, Phys. Rev. B **83**, 220402(R) (2011).

[5]J. Mravlje, M. Aichhorn, and A. Georges, Phys. Rev. Lett. **108**, 197202 (2012).

[6]Y. G. Shi, Y. F. Guo, S. Yu, M. Arai, A. A. Belik, A. Sato, K. Yamaura, E. Takayama-Muromachi, H. F. Tian, H. X. Yang, J. Q. Li, T. Varga, J. F. Mitchell, and S. Okamoto, Phys. Rev. B **80**, 161104 (2009).
[7]S. Calder, V. O. Garlea, D. F. McMorrow, M. D. Lumsden, M. B. Stone, J. C. Lang, J.-W. Kim, J. A. Schlueter, Y. G. Shi, K. Yamaura, Y. S. Sun, Y. Tsujimoto, and A. D. Christianson, Phys. Rev. Lett. **108**, 257209 (2012).
[8]J. C. Slater, Phys. Rev. **82**, 538 (1951).
[9]Y. Shi, Y. Guo, S. Yu, M. Arai, A. Sato, A. A. Belik, K. Yamaura, and E. Takayama-Muromachi, J. Am. Chem. Soc. **132**, 8474 (2010).
[10]S. Kawasaki and M. Takano, J. Soild. State. Chem. **145**, 302 (1999).
[11]S. Blundell, *Magnetism in Condensed Matter* (Oxford University Press, 2001).
[12]S. Nimkar, D. D. Sarma, H. R. Krishnamurthy, and S. Ramasesha, Phys. Rev. B **48**, 7355 (1993).
[13]P. Mahadevan, K. Sheshadri, D. D. Sarma, H. R. Krishnamurthy, and R. Pandit, Phys. Rev. B **55**, 9203 (1997).
[14]P. E. Blöchl, Phys. Rev. B **50**, 17953 (1994); G. Kresse and D. Joubert, *ibid.* **59**, 1758 (1999).
[15]G. Kresse and J. Furthmüller, Phys. Rev. B **54**, 11169 (1996); Comput. Mater. Sci. **6**, 15 (1996).
[16]P. Mahadevan, F. Aryasetiawan, A. Janotti, and T. Sasaki, Phys. Rev. B **80**, 035106 (2009).
[17]L. Vaugier, H. Jiang, and S. Biermann, arXiv:1206.3533v1.
[18]J. C. Slater and G. F. Koster, Phys. Rev. **94**, 1498 (1954).
[19]L. F. Mattheiss, Phys. Rev. B **2**, 3918 (1970).
[20]J. S. Griffith, *The Theory of Transition-Metal Ions* (Cambridge University Press, Cambridge, 1961).
[21]F. M. F. de Groot, J. C. Fuggle, B. T. Thole, and G. A. Sawatzky, Phys. Rev. B **42**, 5459 (1990); P. Mahadevan and D. D. Sarma, *ibid.* **59**, 1739 (1999); **61**, 7402 (2000).
[22]D. Landau and K. Binder, *A Guide to Monte Carlo Simulations in Statistical Physics* (Cambridge University Press, Cambridge, England, 2000).
[23]N. Metropolis, A. Rosenbluth, M. Rosenbluth, A. Teller, and E. Teller, J. Chem. Phys. **21**, 1087 (1953).
[24]P. Mahadevan, N. Shanthi, and D. D. Sarma, Phys. Rev. B **54**, 11199 (1996).
[25]J. E. Hirsch, Phys. Rev. B **31**, 4403 (1985).
[26]From a fitting of the spin-polarized *ab initio* band structure, J_h for Tc is determined to be 0.3 eV.
[27]G. J. Thorogood, M. Avdeev, M. L. Carter, B. J. Kennedy, J. Ting, and K. S. Wallwork, Dalton Trans. **40**, 7228 (2011).
[28]S. V. Halilov, H. Eschrig, A. Y. Perlov, and P. M. Oppeneer, Phys. Rev. B **58**, 293 (1998).
[29]C. Keller and B. Kanellakopulos, J. Inorg. Nucl. Chem. **27**, 787 (1965).
[30]H. Shaked, J. D. Jorgensen, O. Chmaissem, S. Ikeda, and Y. Maeno, J. Solid State Chem. **154**, 361 (2000).
[31]A. P. Mackenzie and Y. Maeno, Rev. Mod. Phys. **75**, 657 (2003).
[32]M. Braden, G. André, S. Nakatsuji, and Y. Maeno, Phys. Rev. B **58**, 847 (1998).